Article

Modeling of the Minimum Fluidization Velocity and the Incipient Fluidization Pressure Drop in a Conical Fluidized Bed with Negative Pressure

Sheng Fang [1,2], Yanding Wei [1,2,*], Lei Fu [3] , Geng Tian [1,2] and Haibin Qu [4,*]

[1] The State Key Laboratory of Fluid Power and Mechatronic Systems, College of Mechanical Engineering, Zhejiang University, Hangzhou 310027, China; fangsheng@zju.edu.cn (S.F.); IamTianGeng@zju.edu.cn (G.T.)

[2] Key Laboratory of Advanced Manufacturing Technology of Zhejiang Province, College of Mechanical Engineering, Zhejiang University, Hangzhou 310027, China

[3] College of Mechanical Engineering, Zhejiang University of Technology, Hangzhou 310023, China; fulei@zjut.edu.cn

[4] Pharmaceutical Informatics Institute, College of Pharmaceutical Sciences, Zhejiang University, Hangzhou 310058, China

* Correspondence: weiyd@zju.edu.cn (Y.W.); quhb@zju.edu.cn (H.Q.); Tel.: +86-571-8795-3851 (Y.W.); +86-571-8820-8428 (H.Q.)

check for updates

Abstract: The modeling of the minimum fluidization velocity (U_{0mf}) and the incipient fluidization pressure drop (ΔP_{mf}) is a valuable research topic in the fluidization field. In this paper, first, a series of experiments are carried out by changing the particle size and material mass to explore their effects on U_{0mf} and ΔP_{mf}. Then, an Ergun equation modifying method and the dimensional analysis method are used to obtain the modeling correlations of U_{0mf} and ΔP_{mf} by fitting the experimental data, and the advantages and disadvantages of the two methods are discussed. The experimental results show that U_{0mf} increases significantly with increasing particle size but has little relationship with the material mass; ΔP_{mf} increases significantly with increasing material mass but has little relationship with the particle size. Experiments with small particles show a significant increase at large superficial gas velocity; we propose a conjecture that the particles' collision with the fluidization chamber's top surface causes this phenomenon. The fitting accuracy of the modified Ergun equation is lower than that of the dimensionless model. When using the Ergun equation modifying method, it is deduced that the gas drag force is approximately 0.8995 times the material total weight at the incipient fluidized state.

Keywords: conical fluidized bed; minimum fluidization velocity; pressure drop; Ergun equation; dimensional analysis

1. Introduction

In the pharmaceutical industry, conical fluidized beds are more widely used than cylindrical fluidized beds because the former have certain advantages [1–3]. First, the particle size distribution can be broad in a granulation/coating process in the pharmaceutical industry. Due to the axial velocity gradient of a conical cylinder, larger particles can be fluidized at the lower layer, while smaller particles can stay at the upper layer without being carried out. Second, the fluidized state of a conical fluidized bed is smoother than that of a cylindrical fluidized bed because the upper layer of the conical cylinder is more extensive and can hold more gas to avoid the slug phenomenon [4]. Except for the unusual shape of the fluidization chamber, most pharmaceutical fluidized beds are negative pressure fluidized beds since the gas-driven equipment (usually a high-pressure fan) is placed at the outlet of the gas

path, which is different from the fluidized beds used in other fields. The reason for this design is that if there is leakage, a negative pressure vessel is safer than a positive pressure vessel, and the material does not scatter everywhere, which would cause contamination.

The gas pressure is one of the essential monitored parameters in a fluidized bed [5]. Through analysis of the gas pressure signal, workers can know whether the fluidized bed is in a normal working state. The gas pressure drop (ΔP) between the surface and the bottom of the material is always used to determine the flow regimes. When the superficial gas velocity (U_0) is low (the subscript "0" in this paper refers to the bottom section of the conical cylinder), the bed is in a static state, and ΔP increases with an increase in U_0; when U_0 reaches a certain velocity, ΔP stops increasing and maintains a relatively stable value. This stable value is called the incipient fluidization pressure drop (ΔP_{mf}) [6], and the corresponding U_0 at this point is called the minimum fluidization velocity (U_{0mf}). U_{0mf} and ΔP_{mf} are of great importance in fluidized bed operation, and many factors affect these two values, among which particle size and material mass are fundamental and essential factors.

Because the experimental methods to obtain U_{0mf} and ΔP_{mf} under specified operating conditions are time-consuming and laborious, many scholars have tried to obtain modeling correlations suitable for general or specific working conditions [7]. In recent years, the proposed modeling correlations can be divided into two categories [8]: one is based on modifying the Ergun equation, and the other is based on dimensional analysis. The Ergun equation was proposed by Sabri Ergun in 1952 [9] to calculate the pressure drop when a gas flows through a packed material [10], and the specific equation is as follows:

$$\frac{dP}{dh} = C_1 \frac{(1-\varepsilon)^2}{\varepsilon^3} \frac{\mu U_h}{(\phi d_P)^2} + C_2 \frac{(1-\varepsilon)}{\varepsilon^3} \frac{\rho_g U_h^2}{\phi d_P} \tag{1}$$

The Ergun equation has high accuracy due to the introduction of parameters such as particle size, particle sphericity, and voidage, so it has been widely accepted and verified. In this equation, C_1 is the coefficient of the viscosity term, and C_2 is the coefficient of the inertial term. For the original Ergun equation, $C_1 = 150$ and $C_2 = 1.75$. Both C_1 and C_2 are empirical values, and many factors, such as equipment size/shape, the friction coefficient, and particle size distribution, may lead to inaccurate prediction results [11]. In 1966, Wen and Yu [12] proposed an empirical model based on the Ergun equation and fitting the experimental data, the specific correlation of which was:

$$\mathrm{Re}_{mf} = \sqrt{33.7^2 + 0.0408 \mathrm{Ar}} - 33.7 \tag{2}$$

In 1982, Grace J.R. [13] argued that replacing the number 33.7 with 27.2 in Equation (2) is most suitable for the gas-solid system. Gibson I.A. [14] et al. also did an in-depth discussion of Wen and Yu's equation.

For a conical fluidized bed, the original Ergun equation cannot be directly used because of the gas velocity gradient in the axial direction, which makes the pressure drop rate vary in the axial direction. To solve this problem, Peng and Fan [15] developed a model to calculate ΔP of a conical liquid–solid fluidized bed by integrating the pressure drop rates of different layers. Jing et al. [16,17] proposed a correlation based on the Ergun equation to calculate U_{0mf} and ΔP_{mf} of a conical fluidized bed using a mathematical processing method similar to Peng and Fan's model. Rachadaporn Kaewklum et al. [18] used Peng and Fan's model to predict U_{0mf} and ΔP_{mf} for air–sand conical beds, and the effects of the sand particle size, cone angle, and static bed height on the flow behavior were discussed. Andrei Koekemoer et al. [19] put forward a method of modifying the coefficients C_1/C_2 in Equation (1) to increase the prediction accuracy, which is adopted and improved in this paper. In this study, we use regression analysis to try to obtain a better combination of C_1 and C_2 that is more suitable for the working conditions of this study.

Dimensional analysis is a widely used modeling method that only pays attention to the mathematical relationships between independent variables and dependent variables while ignoring the physical laws between physical parameters. A dimensionless model has a unified and straightforward

equation form that is composed of a series of dimensionless groups. The general equation form is as follows:

$$\pi_0 = \pi_1^{p_1} \cdot \pi_2^{p_2} \cdot \pi_3^{p_3} \cdots \pi_n^{P_n} \tag{3}$$

where $\pi_0, \pi_1, \ldots, \pi_n$ are all dimensionless groups and $P_1, P_2, \ldots, P_n$ are the exponents of these dimensionless groups. Since the dimension of a dimensionless group is 1, no matter what the exponents are, the equation can satisfy the principle of dimensional harmony. The main difficulty of this method is determining the dimensionless groups, which requires knowing which factors affect the dependent variables. The value of each component can be determined by linear regression or nonlinear regression of the experimental data. Based on selecting appropriate dimensionless groups, a dimensionless model generally achieves higher accuracy under specific working conditions.

Sau et al. [20–22] used the dimensional analysis method to develop modeling correlations for U_{0mf}, ΔP_{mf}, and the bed expansion ratio of conical beds for different kinds of fluidization materials. Khani [23] proposed a dimensionless model using the term $\cos(\alpha)$ instead of $\sin(\alpha)$ compared with Sau's model [20], considering that $\sin(\alpha)$ approaches zero for mini-tapered beds, which may lead to an incorrect prediction result. Mojtaba Rasteh et al. [24] thoroughly considered the effect of PSD (particle size distribution) on U_{0mf} and proposed different correlations for different PSDs (Gaussian/flat/binary). Because the dimensional analysis method has strong applicability, it has been used by many scholars to derive modeling correlations in the field of fluidized bed [25–31]. Some of the correlations proposed by other scholars are listed in Table 1.

Table 1. Correlations proposed by other scholars for predicting U_{0mf} and ΔP_{mf}.

Scholars	Correlations
Sau, D.C. et al. [20]	$\mathrm{Fr} = 0.2714(\mathrm{Ar})^{0.3197} (\sin\alpha)^{0.6092} \left(\frac{\varepsilon_0}{\phi}\right)^{-0.6108}$ $\Delta P_{mf} = 7.457\left(\frac{D_1}{D_0}\right)^{0.038}\left(\frac{d_p}{D_0}\right)^{0.222}\left(\frac{H_0}{D_0}\right)^{0.642}\left(\frac{\rho_s}{\rho_g}\right)^{0.723}$
Khani, M.H. [23]	$\mathrm{Re}_{mf} = 7.16(\mathrm{Ar})^{0.393}\left(\frac{d_p}{D_0}\right)^{0.987}\left(\frac{\varepsilon_0}{\phi}\right)^{-0.833}(\cos\alpha)^{-275.486}, 0 \leq \alpha \leq 4.5°$ $\mathrm{Re}_{mf} = 10.396(\mathrm{Ar})^{0.367}\left(\frac{d_p}{D_0}\right)^{0.889}\left(\frac{\varepsilon_0}{\phi}\right)^{-0.731}(\cos\alpha)^{-10.437}, \alpha > 4.5°$ $\frac{\Delta P_{mf}}{\rho_s g H_s} = 106.729\left(\frac{\rho_s}{\rho_g}\right)^{-0.522}\left(\frac{d_p}{D_0}\right)^{0.309}\left(\frac{H_0}{D_0}\right)^{-0.379}(\cos\alpha)^{-10.858}, 0 \leq \alpha \leq 4.5°$ $\frac{\Delta P_{mf}}{\rho_s g H_s} = 163.419\left(\frac{\rho_s}{\rho_g}\right)^{-0.524}\left(\frac{d_p}{D_0}\right)^{0.269}\left(\frac{H_0}{D_0}\right)^{-0.976}(\cos\alpha)^{-3.277}, \alpha > 4.5°$
Rasteh Mojtaba et al. [24]	$\mathrm{Re}_{mf} = 0.254(\mathrm{Ar})^{0.585}\left(\frac{\varepsilon_0}{\phi}\right)^{3.12}\left(\frac{H_0}{D_0}\right)^{0.264}\left(\frac{d_p}{D_0}\right)^{0.0016}(\cos\alpha)^{-13.2}$

However, in the literature related to the modeling of U_{0mf} and ΔP_{mf}, most of the research equipment that was used was positive pressure cylindrical fluidized beds. Due to the differences in the gas path structure and the fluidization chamber shape, the previous research results cannot be directly applied to negative pressure conical fluidized beds. In addition, both the method based on modifying the Ergun equation and the method based on dimensional modeling have characteristics, advantages, and disadvantages, while few studies have compared these two methods. Based on these problems, we have carried out this study. The innovations of this study lie in the following: (a) the flow behaviors of the negative pressure conical fluidized bed are studied, (b) the Ergun equation modifying method and the dimensional analysis method are both used and compared, and (c) this study proposes the inference that the total gas drag force is 0.8995 times the particles' gravity in the initial stage of fluidization. In this study, first, a series of experiments are carried out, and U_{0mf} and ΔP_{mf} are obtained as experimental empirical data; the effects of material mass and particle size on U_{0mf} and ΔP_{mf} are discussed. Second, we separately use the above two methods to fit the empirical data and derive models of U_{0mf} and ΔP_{mf}; by using these modeling correlations, workers can quickly determine U_{0mf} and ΔP_{mf} based on some variables, and then determine the production parameters. Finally, the prediction

ability of the proposed correlations and the characteristics of the two modeling methods are discussed, which can be used as a reference for selecting an appropriate method in practical application.

2. Experimental Section

2.1. Experimental Equipment

As shown in Figure 1, in this study, a pharmaceutical granulation/drying fluidized bed (FBL-10, Xiaolun Pharmaceutical Machinery, Wenzhou, China) was used, which was a negative pressure conical fluidized bed. The conical cylinder was detachable with a bottom diameter of 180 mm and a top diameter of 300 mm, and the cross-sectional area was round; the conical angle $\alpha = 8.88°$. There was a distribution plate made of stainless steel with a thickness of 3 mm for supporting materials and ventilation. The holes on the distribution plate were arranged in a square array mode, the diameter of each hole was 1.6 mm, and the total number of holes was 1617, so the overall opening ratio was 12.78%. A double-layer fine screen covered the distribution plate to prevent fine materials from falling through the holes and to force the airflow to be uniformly distributed. A high-pressure fan (2RB-730N-7AH26, Gzling Mechanical & Electrical Equipment, Wuxi, China) was placed at the outlet of the gas path, so the pressure in the fluidization chamber was negative with respect to the ambient pressure. The high-pressure fan had a rated power of 3 kW and could generate a maximum negative pressure of −22 kPa. The power of the fan was controlled by a frequency converter (ATV310HU30N4, Schneider Electric SA, Paris, France); thus, the gas velocity could be changed. The control range of the fan power was 1–100%, and the minimum control interval was 1%. The ambient pressure was standard atmospheric pressure, the air humidity was controlled by a humidity controller (MDH-40Y, Senjing Motor Manufacturing, Hangzhou, China) to 50–60%, and the ambient temperature was controlled via air conditioning to 25 °C ± 1 °C.

A vortex flowmeter (DN100, Meikong Automation Technology, Hangzhou, China) was connected in series at the exhaust pipe to measure the flowrate with an accuracy of 1%. Two air pressure measurement ports were set in the center of the plenum and the front of the filter bag, named P1 and P2, respectively. Two identical high-precision air pressure sensors were connected to the measurement ports, and the measurement range was −10 kPa–10 kPa with an accuracy of 0.5%. The pressure sensors' signals were sampled by a high-speed data acquisition card (USB-6009, National Instruments, Austin, TX, USA) with a sampling frequency of 40 Hz. The pressure transfer hose (not shown in Figure 1) had a length of 100 mm and an inner diameter of 4 mm, so the transmission time delay of the pressure fluctuations in the hose could be ignored [32].

Micro glass beads were used as fluidized materials in this study, which are nonporous particles. The true density of these particles was 2409 ± 8.8 kg/m^3, measured by the drainage method. Using different screen combinations, we screened out a total of 5 kinds of materials with different particle sizes, which were numbered #1, #2, #3, #4, and #5. The average diameter (randomly measuring the diameters of 50 particles and taking the average) and sphericity (replaced by the circularity of the projection photo) of each kind of particle were determined by a digital microscope (GP-660V, Gaopin Precision Instruments, Shanghai, China), and the natural bulk voidage of each kind of particle was measured by a bulk density meter (XF-16913, LICHEN-BX Instrument Technology, Shanghai, China), as shown in Table 2. Since the screen size range of each kind of particles was relatively narrow, the particle distributions of all kinds of particles were considered a typical narrow distribution. The microscopic photograph of the experimental particles is shown in Figure 2, and the bright spots on the particles in the photograph are caused by the microscope's illumination light.

Table 2. Physical properties of materials and Geldart particle type.

| Material Number	#1	#2	#3	#4	#5
Screen size range (mm)	0.653–0.855	0.527–0.653	0.377–0.527	0.177–0.265	0.140–0.177
Particle diameter (mm)	0.744 ± 0.061	0.632 ± 0.046	0.454 ± 0.046	0.235 ± 0.025	0.164 ± 0.015
Bulk density (kg/m^3)	1579 ± 2.1	1498 ± 2.7	1500 ± 2.3	1420 ± 0.5	1471 ± 3.3
Static voidage (-)	$0.344 ± 1.7 \times 10^{-3}$	$0.378 ± 2.0 \times 10^{-3}$	$0.377 ± 1.9 \times 10^{-3}$	$0.410 ± 1.6 \times 10^{-3}$	$0.389 ± 2.2 \times 10^{-3}$
Sphericity (-)	0.979 ± 0.031	0.966 ± 0.055	0.970 ± 0.058	0.903 ± 0.162	0.992 ± 0.037
Angle of repose (°)	24.1 ± 0.23	23.3 ± 0.15	26.2 ± 0.11	24.3 ± 0.30	23.8 ± 0.12
Hausner ratio (-)	$1.011 ± 0.8 \times 10^{-3}$	$1.039 ± 1.1 \times 10^{-3}$	$1.035 ± 0.3 \times 10^{-3}$	$1.077 ± 0.8 \times 10^{-3}$	$1.058 ± 0.3 \times 10^{-3}$
Material mass (kg)	2/2.5/3/3.5/4	2/2.5/3/3.5/4	2/2.5/3/3.5/4	2/2.5/3/3.5/4	2/2.5/3/3.5/4
Geldart particle type (-)	D	B	B	B	B
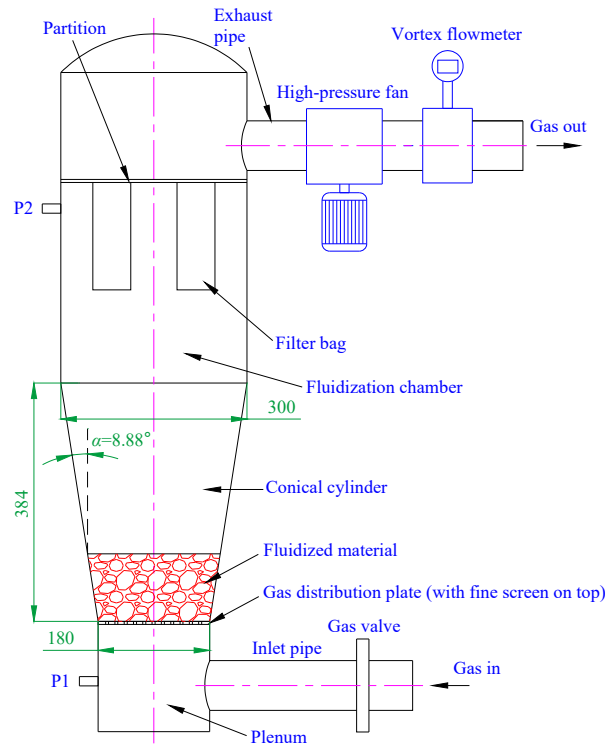
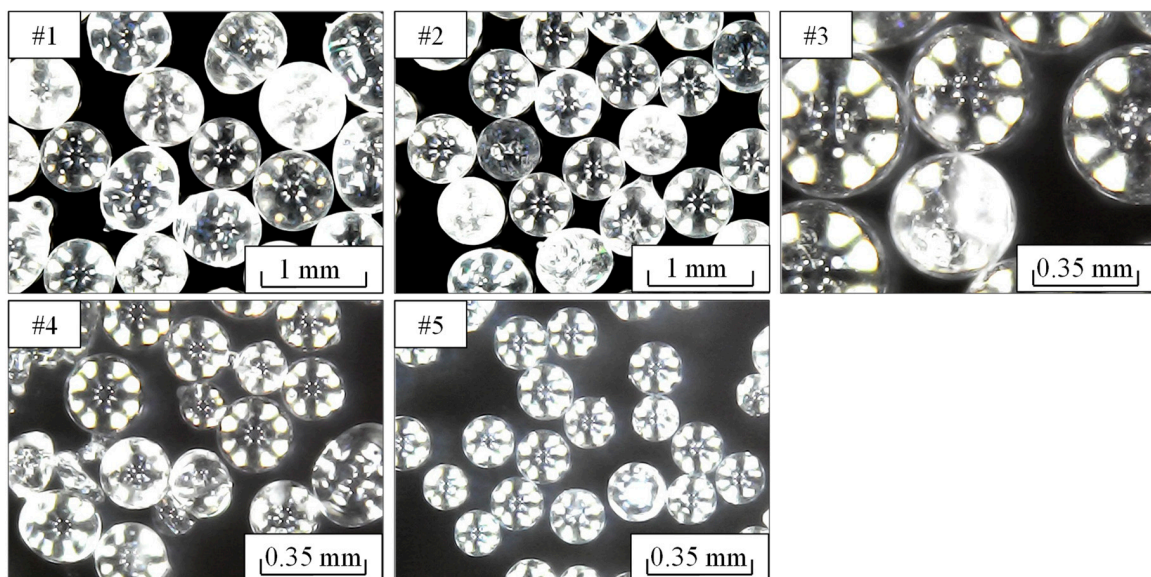**Figure 1.** Schematic diagram of the experimental equipment.

Figure 2. Microscopic photograph of experimental particles.

According to the Geldart classification method [33], #1 was class D particles, and #2–#5 were class B particles, where #2 was very close to the BD boundary. According to common knowledge in the field of fluidization, the main characteristic of class B and D particles is that there is no obvious expansion before the fluidization occurs. Additionally, the minimum bubbling velocity and the minimum fluidization velocity are the same; in other words, there is almost no particulate fluidization process in the fluidized bed.

2.2. Experimental Design and Procedure

Since port P1 is below the distribution plate, the pressure difference between ports P1 and P2 includes the pressure drop caused by the distribution plate. However, ΔP refers to the pressure drop between the top and bottom sections of the material, so it is necessary to obtain the pressure drop caused by the distributor first. For this reason, we first carried out a separate experiment in which there was no material in the fluidized bed, and the number of this experiment was 00.

In this study, a total of 5 kinds of material masses were set to 2/2.5/3/3.5/4 kg. The five kinds of material masses were cross-combined with the five kinds of particle sizes, and therefore, a total of 25 experiments were developed. The experimental numbers are given in Table 3. For example, in experiment 14, #3 particles with a mass of 3.5 kg were used as the experimental material.

Table 3. Experimental number correspondence table.

Material Number	Experimental Number				
	Material Mass 2 kg	Material Mass 2.5 kg	Material Mass 3 kg	Material Mass 3.5 kg	Material Mass 4 kg
#1	01	02	03	04	05
#2	06	07	08	09	10
#3	11	12	13	14	15
#4	16	17	18	19	20
#5	21	22	23	24	25

The experimental steps of experiments 01–25 were as follows: starting from a fan power opening (called fan opening hereafter) of 70%, decrease the fan opening by 1% each time. After the fluidized state is stable, record the signals (x_{P1}, x_{P2}, x_f) for 30 s. Repeat the above operations until the fan power reaches 11%. Each experiment was repeated three times, and the most credible set of data was selected as the final data during data screening. To ensure that all experiments were carried out under the same conditions, before each experiment, the distribution plate, double-layer screen, and filter bag were cleaned, and the equipment was prefluidized at 50% fan power for 15 min to keep the material in a dry and loose state. For experiment 00, the fan power stopped at 0%; the rest of the procedure was the same as that in experiments 01–25.

3. Signal Processing Methods

This paper ignores the influence of gas compression and considers the gas flow rate at any cross section of the conical cylinder to be the same. The superficial gas velocity at any section is calculated using the following equations:

$$U_h = \bar{x}_f / S_h \tag{4}$$

$$U_0 = \bar{x}_f / S_0 \tag{5}$$

where $\bar{x}_f$ is the average value of the flow rate time-series signal (x_f) and S_h is the sectional area of the conical cylinder at the height of h.

The number of the empty bed experiment is 00, and the relationships among the fan opening, U_0, and ΔP_p are shown in Figure 3. As shown in Figure 3, with an increase in the fan opening, U_0 and ΔP_p continue to increase.

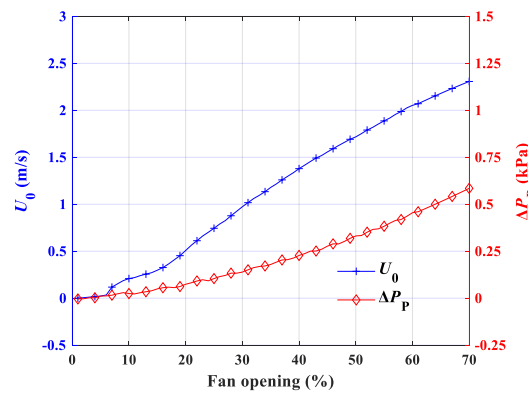**Figure 3.** U_0 and ΔP_P at different fan openings in the empty bed experiment (number 00).

As shown in Equation (6), by subtracting the average values of x_{P1} and x_{P2} in the empty bed experiment (material mass $W = 0$), the pressure drop generated by the gas distribution plate (ΔP_P) can be calculated. For each fan opening, ΔP_P and U_0 were recorded so that the mapping relationship between a series of ΔP_P and a series of U_0 can be established. Therefore, for a given U_0, the value of ΔP_P can be determined by this mapping relationship. As shown in Equation (7), for experiments 01–25, by subtracting the average values of x_{P1} and x_{P2} and then subtracting ΔP_P (under the current U_0), ΔP can be obtained.

$$\Delta P_\mathrm{P} = (\overline{x}_{\mathrm{P1}} - \overline{x}_{\mathrm{P2}})|_{W=0} \ \text{(empty bed experiment, number 00)} \tag{6}$$

$$\Delta P = \overline{x}_{\mathrm{P1}} - \overline{x}_{\mathrm{P2}} - \Delta P_\mathrm{P}\big|_{U_0} \ \text{(experiment 01–25)} \tag{7}$$

The intersection method is used to determine $U_{0\mathrm{mf}}$ and ΔP_mf. The specific determination process is as follows. first determine an inflection point, and from the second point before the inflection point, take as many points as possible near a straight line to fit the first straight line; then, from the second point after the inflection point, take 4–6 continuous points, then plot a horizontal straight line as the second line, whose height is the average of the taken points' ordinate values; the intersection point of the two straight lines is considered to be the point ($U_{0\mathrm{mf}}$, ΔP_mf). Take experiment 06 shown in Figure 4 as an example. The two black lines in Figure 4 are the two straight lines, and $U_{0\mathrm{mf}}$ and ΔP_mf are the abscissa and ordinate of the intersection point, respectively.
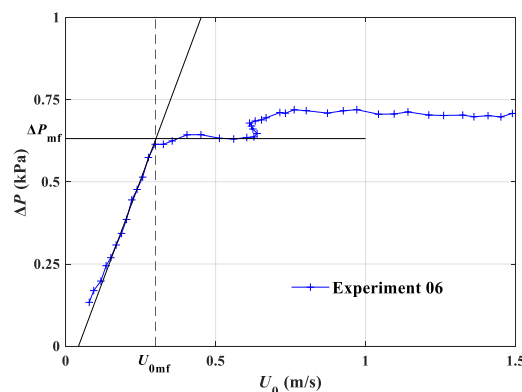
Figure 4. Schematic diagram of the $U_{0\mathrm{mf}}$ and ΔP_mf measurement method.

In this paper, the root mean square error (RMSE) and R^2 are used to describe the fitting accuracy quantitatively. RMSE means the root mean square error; the smaller the value, the closer the fitting

value is to the actual value. R^2 is the determination coefficient, and its value is between 0 and 1. The higher the value is, the higher the fitting accuracy.

$$\text{RMSE} = \sqrt{\frac{1}{N}\sum_{i=1}^{N}(x_i - \hat{x}_i)^2} \tag{8}$$

$$R^2 = 1 - \frac{\sum\limits_{i=1}(x_i - \hat{x}_i)^2}{\sum\limits_{i=1}(x_i - \overline{x})^2} \tag{9}$$

4. Results and Discussion

4.1. Effects of Material Mass and Particle Size on Flow Behavior

As shown in Figure 5, the 2nd row and 2nd column of the data in Table 3 are taken to display the effect of the material mass and the particle size on the flow behavior, and the experimental numbers are 06/07/08/09/10 and 02/07/12/17/22, respectively. A series of vertical dotted lines on the left side of Figure 5 represent U_{0mf} of each experiment, and their colors and markers are the same as those of the curves of the corresponding experiments.
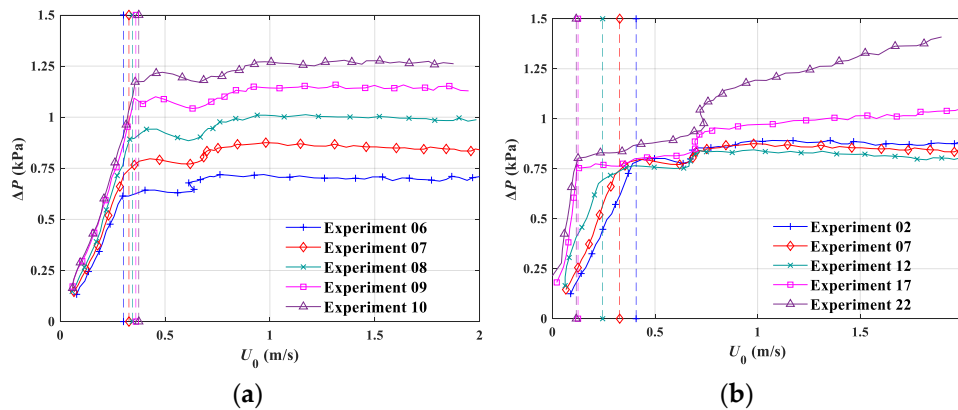

Figure 5. ΔP at different U_0 values of (**a**) the 2nd row and (**b**) the 2nd column of experiments in Table 3.

As shown in Figure 5a, when $U_0 < U_{0mf}$, with an increase in U_0, ΔP continues to increase linearly; when $U_0 > U_{0mf}$, ΔP stops growing and enters a stable stage. In addition, the higher the material mass, the greater ΔP_{mf} is. The material mass has little effect on U_{0mf}; with an increase in the material mass, U_{0mf} increases slightly. As shown in Figure 5b, when $U_0 < U_{0mf}$, the particles with a larger particle size have a lower growth rate. When $U_0 > U_{0mf}$, the experiments have similar ΔP_{mf} values. When U_0 reaches a certain velocity, experiments 17/22 show significant ΔP growth, while the other experiments show little or no increase. We suppose the possible reason is as follows. When the gas velocity is high enough, the fine particles move to the upper part of the fluidized chamber and collide with the top surface. Assuming that all the particles are a whole body, this whole body is now subjected to the downward gravity force and the downward support force exerted by the top surface, so the pressure drop continues to increase because the required gas flow drag force becomes larger. For experiments with larger particle sizes (experiment 02/07/12), the particles cannot be brought high enough to collide with the top surface. Particle size has a significant influence on U_{0mf}; as the particle size increases, U_{0mf} increases significantly.

U_{0mf} and ΔP_{mf} obtained in all experiments are shown in Table 4. 3D views of the particle size and material mass versus U_{0mf} and ΔP_{mf} are plotted to facilitate the observation of the variation regularity in Figure 6.

Table 4. U_{0mf} and ΔP_{mf} of each experiment.

Material Number	U_{0mf} (m/s) ΔP_{mf} (kPa)				
	Material Mass 2 kg	Material Mass 2.5 kg	Material Mass 3 kg	Material Mass 3.5 kg	Material Mass 4 kg
#1	0.403	0.408	0.413	0.419	0.433
	0.650	0.810	0.964	1.064	1.213
#2	0.302	0.328	0.344	0.361	0.375
	0.640	0.793	0.933	1.093	1.213
#3	0.232	0.245	0.249	0.255	0.258
	0.615	0.756	0.903	1.043	1.170
#4	0.106	0.125	0.136	0.149	0.157
	0.643	0.771	0.899	1.020	1.116
#5	0.113	0.116	0.125	0.134	0.143
	0.665	0.829	0.966	1.117	1.189

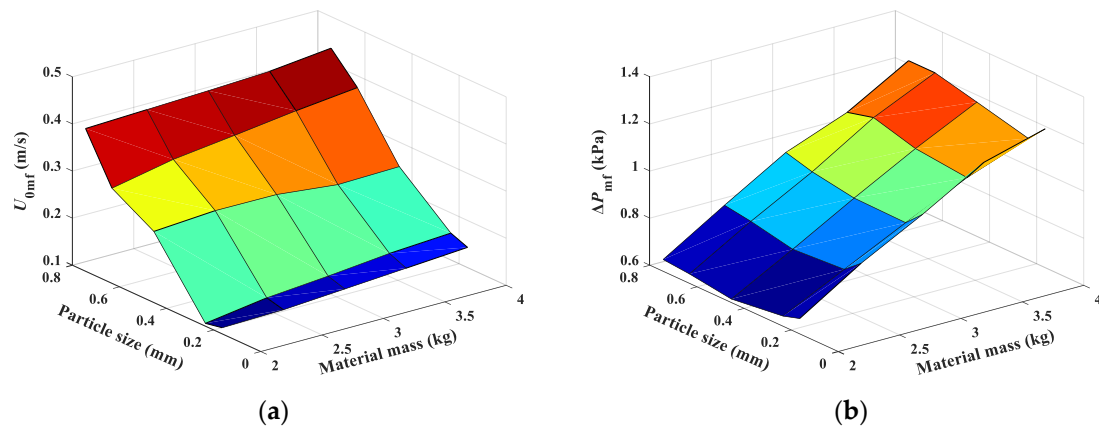(**a**)   (**b**)

Figure 6. 3D views of the particle size and material mass versus (**a**) U_{0mf} and (**b**) $\Delta P_{mf.}$

Table 4 and Figure 6 show that for U_{0mf}, the main influencing factor is the particle size; the larger the particle size, the larger U_{0mf} is. The influence of the material mass is small, and U_{0mf} increases slightly with an increase in the material mass. For ΔP_{mf}, the main influencing factor is the material mass, and ΔP_{mf} is approximately proportional to the material mass. The influence of the particle size is small and complex; for the same material mass, ΔP_{mf} of #1–#4 particles is almost the same, and ΔP_{mf} of #5 particles is 2–13% larger than the former.

4.2. Mathematical Modeling

4.2.1. Ergun Equation Modifying Method

The fluidized state could be observed through the glass window embedded in the sidewall of the conical cylinder, and the expansion of the bed surface could be clearly observed with the help of a thin film ruler that was pasted on the inner wall of the conical cylinder. When $U_0 < U_{0mf}$, the bed was in a fixed state. When U_0 approached U_{0mf}, slight expansion could be observed in the bed, and the bed height expansion ratio was approximately 2%. After U_0 reached U_{0mf}, bubbling was observed in the central part of the bed surface. As U_0 continued to increase, significant bubbling occurred throughout the entire cross section, and the fluidization height also increased as more particles were brought into the freeboard.

To simplify the model, the following assumptions are made for the point at which $U_0 = U_{0mf}$: the material expands uniformly, the bed height expansion ratio in the height direction is 2%, and the surface of the bed is flat.

From Equations (4) and (5), it can be further deduced that U_h is the function value of r_h, and the deduced equation is as follows:

$$U_h = U_0 \frac{S_0}{S_h} = U_0 \frac{r_0^2}{r_h^2} \tag{10}$$

As Figure 7 shows, according to the trigonometric function equation:

$$r_h = r_0 + h\tan(\alpha) \tag{11}$$
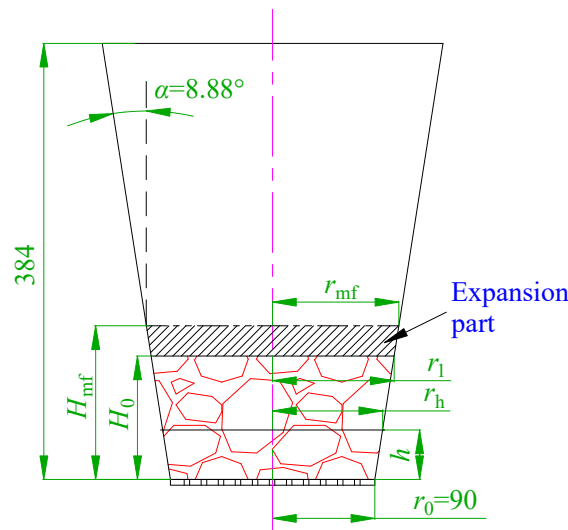
$$r_1 = r_0 + H_0\tan(\alpha) \tag{12}$$

Figure 7. Schematic diagram of the dimensional parameters of the conical cylinder.

To obtain a precise H_0 value for each experiment in Table 3, the following equation is drawn based on the relationship of volume times density is equal to mass:

$$\frac{1}{3}H_0\pi(r_0^2 + r_0r_1 + r_1^2)(1 - \varepsilon_0)\rho_s = W \tag{13}$$

By solving the combined equations of Equations (12) and (13), the H_0 value can be obtained. In this study, an exhaustive method is used, and the programming and calculation are conducted in MATLAB. The specific method is to assign all the values of every 0.0001 in 0–0.1 to H_0 (unit: m) and substitute H_0 into Equations (12) and (13); then, calculate the equation error of Equation (13); finally, the best-matched H_0 value can be obtained by finding the minimum absolute equation error. The calculated H_0 values of all experiments are listed in Appendix A.

Since the bed expansion ratio is 2%, H_{mf}, r_{mf}, and ε_{mf} can be determined by the following equations:

$$H_{mf} = 1.02H_0 \tag{14}$$

$$r_{mf} = r_0 + H_{mf}\tan(\alpha) \tag{15}$$

$$\varepsilon_{mf} = 1 - \frac{W}{\rho_s\pi H_{mf}(r_0^2 + r_0r_{mf} + r_{mf}^2)/3} \tag{16}$$

Under the condition of $U_0 = U_{0mf}$, the original Ergun equation is as follows:

$$\frac{dP}{dh} = 150\frac{(1 - \varepsilon_{mf})^2}{\varepsilon_{mf}^3}\frac{\mu U_h}{(\phi d_P)^2} + 1.75\frac{(1 - \varepsilon_{mf})}{\varepsilon_{mf}^3}\frac{\rho_g U_h^2}{\phi d_P} \tag{17}$$

Set $A = 150\frac{(1-\varepsilon_{mf})^2}{\varepsilon_{mf}^3}\frac{\mu}{(\phi d_P)^2}$ and $B = 1.75\frac{(1-\varepsilon_{mf})}{\varepsilon_{mf}^3}\frac{\rho_g}{\phi d_P}$ so that Equation (17) can be simplified to:

$$\frac{dP}{dh} = AU_h + BU_h^2 \tag{18}$$

The drag force of the gas on the particles is:

$$dF = dP \cdot S_h \tag{19}$$

Integrate the left and right sides of Equation (19) to h at the same time with an integral interval of $0\text{-}H_{mf}$, and simplify it as follows:

$$
\begin{aligned}
F_{mf} &= \int_0^{H_{mf}} \left(AU_{0mf}\frac{r_0^2}{(r_0+h\tan\alpha)^2} + BU_{0mf}^2\frac{r_0^4}{(r_0+h\tan\alpha)^4} \right)\pi(r_0+h\tan\alpha)^2 dh \\
&= \pi r_0^2 H_{mf}\left(AU_{0mf} + BU_{0mf}^2\frac{r_0}{r_{mf}} \right)
\end{aligned} \tag{20}
$$

Since the inner wall of the conical cylinder is relatively smooth, the friction force of the wall against the particles can be ignored. According to previous studies [15,16], when $U_0 = U_{0mf}$, the drag force exerted on the particles is equal to the gravity force of the particles; that is:

$$F_{mf} = G \tag{21}$$

Substitute Equation (20) into Equation (21); that is:

$$\pi r_0^2 H_{mf}\left(AU_{0mf} + BU_{0mf}^2\frac{r_0}{r_{mf}}\right) = Wg \tag{22}$$

By solving Equation (22), the calculated U_{0mf} can be obtained. (H_{mf}, r_{mf}, and ε_{mf} can be obtained in advance by Equations (14)–(16), respectively)

Integrate the left and right sides of Equation (18) to h at the same time with an integral interval of $0\text{-}H_{mf}$, and simplify it as follows:

$$
\begin{aligned}
\Delta P_{mf} &= \int_0^{H_{mf}} \left(AU_{0mf}\frac{r_0^2}{(r_0+h\tan\alpha)^2} + BU_{0mf}^2\frac{r_0^4}{(r_0+h\tan\alpha)^4} \right) dh \\
&= AU_{0mf}H_{mf}\frac{r_0}{r_{mf}} + BU_{0mf}^2 H_{mf}\frac{r_0(r_0^2+r_0 r_{mf}+r_{mf}^2)}{3r_{mf}^3}
\end{aligned} \tag{23}
$$

The calculated ΔP_{mf} can be obtained by substituting the calculated U_{0mf} into Equation (23).

For every experiment in Table 3, conduct the above calculation steps to obtain the calculated U_{0mf} and calculated ΔP_{mf} values. To facilitate observation, the experimentally measured values of U_{0mf} and ΔP_{mf} are taken as the abscissa and the calculated values as the ordinate, as Figure 8 shows.

Figure 8 shows that the prediction accuracy of U_{0mf} is relatively high (absolute error < 20%) for the data of experiments 06–10 and very poor for experiments 16–25 in which small particles were used, and all the prediction values are smaller than the experimental values. For the prediction of ΔP_{mf}, the prediction accuracy is high, with similar errors between 0–+20%. Substituting all prediction and experimental values into Equations (8) and (9), the overall RMSE and R^2 can be obtained, as shown in Table 5. There are many possible reasons for the low prediction accuracy: (a) The measured values of some variables, especially the sphericity, are difficult to accurately determine. (b) There may be differences in some environmental parameters compared with the experiments for deducing the Ergun equation, such as gas humidity, which greatly affects the gas viscosity and the drag force. (c) The conical wall may have an upward support force for the material in the initial fluidization stage.
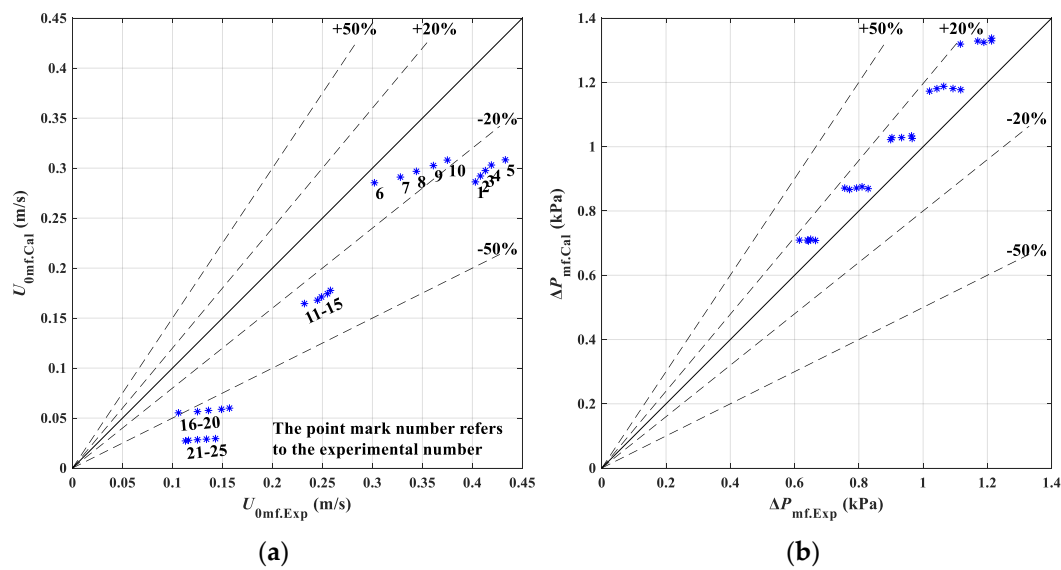
Figure 8. Comparison of the calculated and experimental values of (**a**) U_{0mf} and (**b**) ΔP_{mf} for the original Ergun equation.

Table 5. Coefficients and prediction accuracies of the original and modified Ergun equations.

| | C_1 | C_2 | C_3 | U_{0mf} | | ΔP_{mf} | |
				RMSE (m/s)	R^2 (-)	RMSE (kPa)	R^2 (-)
Original	150	1.75	1	0.0872	0.4209	0.1076	0.6908
Modified	46.61	3.25	0.8995	0.0402	0.8771	0.0291	0.9774

To increase the prediction accuracy of U_{0mf} and ΔP_{mf}, the original coefficients at two sites are changed. The coefficients C_1/C_2 in Equation (1) are changed at the first site, whose original values are 150/1.75, respectively. At the second site, considering that the conical wall may support the material, a multiplicative correction coefficient C_3 is added to Equation (21) as follows:

$$F_{mf} = C_3 \cdot G \tag{24}$$

Therefore, Equation (22) is modified as follows:

$$\pi r_0^2 H_{mf}(AU_{0mf} + BU_{0mf}^2 \frac{r_0}{r_{mf}}) = C_3 \cdot Wg \tag{25}$$

where $A = C_1 \frac{(1-\varepsilon_{mf})^2}{\varepsilon_{mf}^3} \frac{\mu}{(\phi d_P)^2}$ and $B = C_2 \frac{(1-\varepsilon_{mf})}{\varepsilon_{mf}^3} \frac{\rho_g}{\phi d_P}$. Equation (25) is the equation used in the following fitting operations.

All the calculations are performed by MATLAB software, a method of exhaustive optimization is used, and the optimization goal is to minimize the sum of the RMSE values of U_{0mf} and ΔP_{mf} (RMSE$_{sum}$).

The specific calculation processes are shown in Figure 9. First, a preset value of 0.8 is given for C_3, then C_1/C_2 are obtained by fitting the experimental data using a linear regression method ("regress" function in MATLAB). Then, this $C_1/C_2/C_3$ combination is used to calculate the value of RMSE$_{sum}$, and the $C_1/C_2/C_3$ combination and RMSE$_{sum}$ are recorded. Then, add 0.0001 to the previous C_3 preset value, and perform the same calculation and recording for each C_3 preset value. When the C_3 preset value reaches 1.2, the exhaustive optimization calculation is ended. Finally, the $C_1/C_2/C_3$ combination corresponding to the minimum value of RMSE$_{sum}$ is found. The final results are $C_1 = 46.61$, $C_2 = 3.25$, and $C_3 = 0.8995$. The coefficients and modeling accuracies of the original and modified

Ergun equations are listed in Table 5, and the modeling results of the modified Ergun equation are shown in Figure 10.
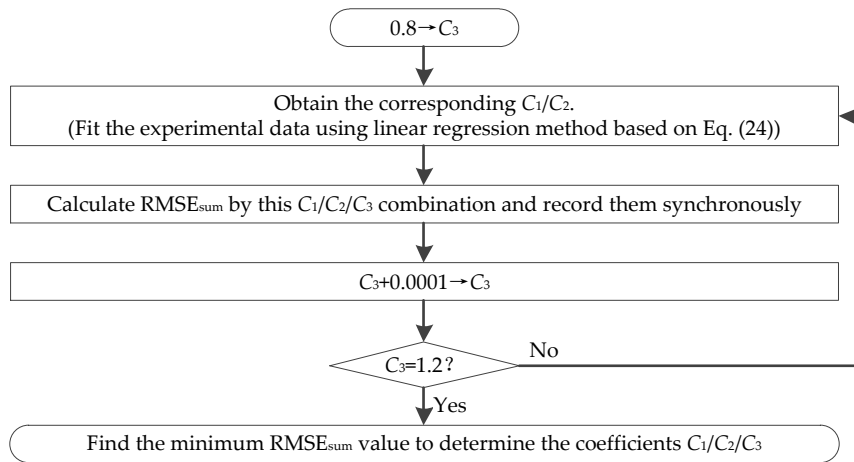

Figure 9. Specific calculation processes to determine the coefficients $C_1/C_2/C_3$.
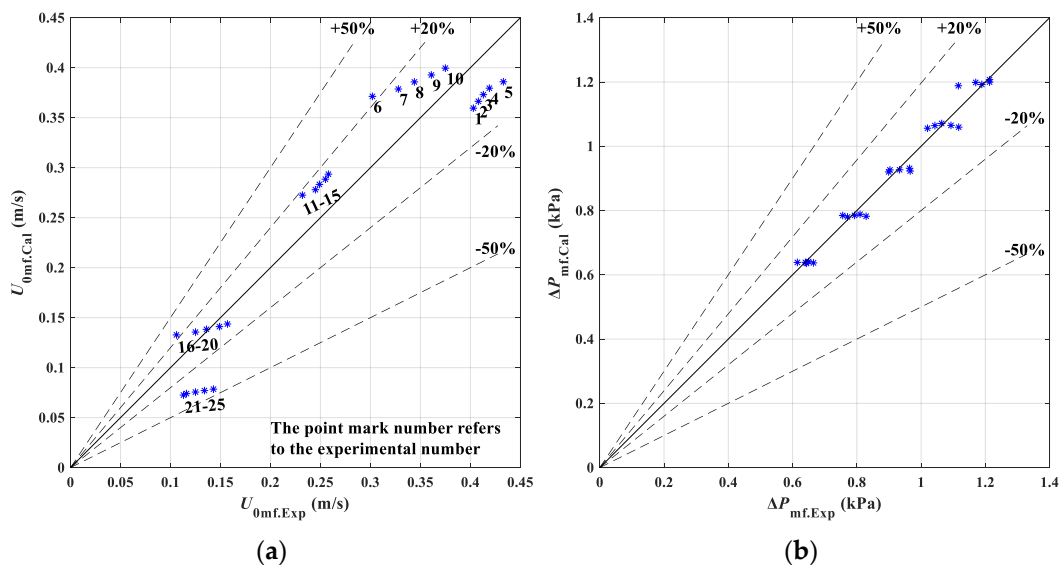

(**a**)   (**b**)

Figure 10. Comparison of the calculated and experimental values of (**a**) U_{0mf} and (**b**) ΔP_{mf} for the modified Ergun equation.

Substitute $C_3 = 0.8995$ into Equation (24), i.e.,

$$F_{mf} = 0.8995 \cdot G \tag{26}$$

We speculate that the reason for Equation (26) is that when fluidization occurs, the conical wall still has support for the particles, which can decompose into an upward component force; therefore, when the drag force of the gas is less than the gravity force of particles (0.8995 < 1), the particles can still be fluidized, and the coefficient C_3 should be related to the cone angle. Some literature has proposed separation models of conical fluidized beds, which may help analyze this problem [34,35]. In future research, we will try to measure the possible supporting force and study the value trend of the coefficient C_3.

To sum up, the specific calculation process of the Ergun equation modifying method is that U_{0mf} can be calculated by solving the following equation:

$$\pi r_0^2 H_{mf}(A\,U_{0mf}+BU_{0mf}^2\frac{r_0}{r_{mf}})=0.8995\cdot Wg \tag{27}$$

where $A=46.6\frac{(1-\varepsilon_{mf})^2}{\varepsilon_{mf}^3}\frac{\mu}{(\phi d_P)^2}$ and $B=3.25\frac{(1-\varepsilon_{mf})}{\varepsilon_{mf}^3}\frac{\rho_g}{\phi d_P}$ (H_{mf}, r_{mf}, and ε_{mf} can be obtained by Equations (14)–(16), respectively). After U_{0mf} is calculated, ΔP_{mf} can be calculated by substituting the calculated U_{0mf} into Equation (23).

4.2.2. Dimensional Analysis

To obtain a dimensionless correlation, we first determine the factors that influence the hydrodynamic behavior of the fluidized bed, which are the particle size (d_P), initial bed height (H_0), bottom diameter (D_0), initial bed voidage (ε_0), particle sphericity (φ), particle true density (ρ_s), gas density (ρ_g), gas viscosity (μ), angle of repose (θ), Hausner ratio (R). These factors are recast into several dimensionless groups containing the Reynolds number ($Re_{mf}=\frac{\rho_g U_{0mf} d_P}{\mu}$), Archimedes number ($Ar=\frac{g d_P^3 \rho_g(\rho_s-\rho_g)}{\mu^2}$), $\frac{\Delta P_{mf}}{\rho_s g H_0}$, $\frac{\varepsilon_0}{\phi}$, $\frac{H_0}{D_0}$, $\frac{d_P}{D_0}$, $\frac{\theta}{R}$, and the correlations among these above dimensionless groups with undetermined coefficients are as follows:

$$Re_{mf}=a_1\cdot(Ar)^{b_1}\cdot\left(\frac{\varepsilon_0}{\phi}\right)^{c_1}\cdot\left(\frac{H_0}{D_0}\right)^{d_1}\cdot\left(\frac{d_P}{D_0}\right)^{e_1}\cdot\left(\frac{\theta}{R}\right)^{f_1} \tag{28}$$

$$\frac{\Delta P_{mf}}{\rho_s g H_0}=a_2\cdot(Ar)^{b_2}\cdot\left(\frac{\varepsilon_0}{\phi}\right)^{c_2}\cdot\left(\frac{H_0}{D_0}\right)^{d_2}\cdot\left(\frac{d_P}{D_0}\right)^{e_2}\cdot\left(\frac{\theta}{R}\right)^{f_2} \tag{29}$$

To obtain the undetermined coefficients of Equations (28) and (29), both linear regression and nonlinear regression methods can be used. For the linear regression method, first, take the logarithm of both sides of Equation (28) as follows:

$$lg(Re_{mf})=lg(a_1)+b_1\cdot lg(Ar)+c_1\cdot lg\left(\frac{\varepsilon_0}{\phi}\right)+d_1\cdot lg\left(\frac{H_0}{D_0}\right)+e_1\cdot lg\left(\frac{d_P}{D_0}\right)+f_1\cdot lg\left(\frac{\theta}{R}\right) \tag{30}$$

Then, the "regress" function in MATLAB can be used to fit the undetermined coefficients, i.e., a_1, b_1, c_1, d_1, e_1, and f_1

For the nonlinear regression method, the "nlinfit" function in MATLAB is used to fit the undetermined coefficients of Equations (28) and (29) directly, and the results of the linear regression are set as the initial values of iteration. The results of the linear and nonlinear regression methods are shown in Tables 6 and 7 and Figure 11. Based on the values of R^2 and RMSE, there is little difference between the fitting accuracy of the linear and nonlinear regression methods, especially for ΔP_{mf}, where the models are almost the same.

Table 6. Results of the linear and nonlinear regression methods of U_{0mf} for the dimensionless model.

	a_1	b_1	c_1	d_1	e_1	f_1	RMSE (m/s)	R^2 (-)
Linear regression	1	0.504	−1.355	0.326	0.236	−0.635	0.011	0.991
Nonlinear regression	1.033	0.509	−1.142	0.186	0.232	−0.645	0.009	0.994

Table 7. Results of the linear and nonlinear regression methods of ΔP_{mf} for the dimensionless model.

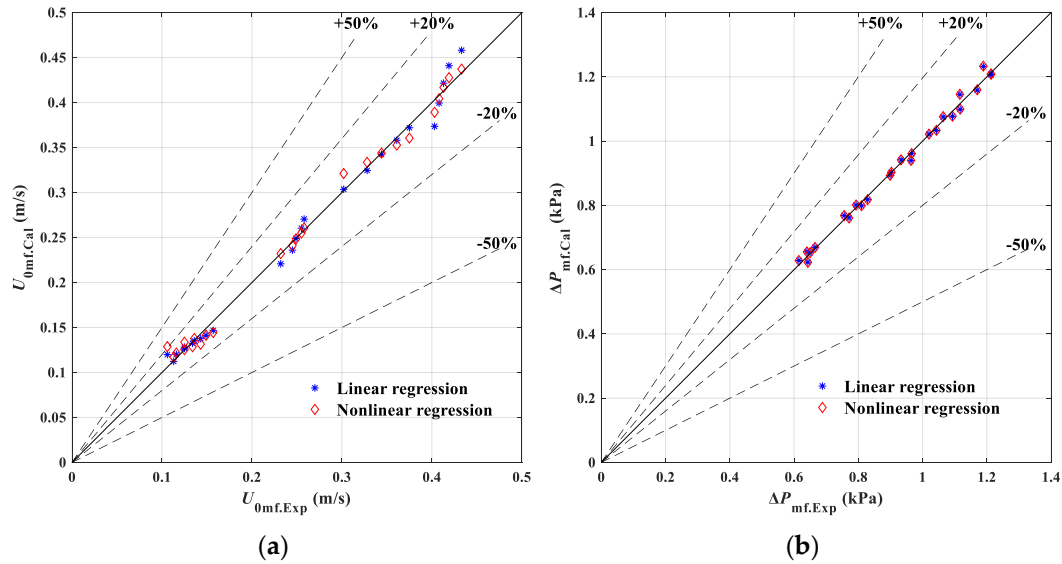|	a_2	b_2	c_2	d_2	e_2	f_2	RMSE (kPa)	R^2 (-)
Linear regression	1	−0.003	−0.642	0.020	0.010	−0.354	0.015	0.994
Nonlinear regression	0.997	−0.003	−0.648	0.017	0.010	−0.352	0.015	0.994

Figure 11. Comparison of the calculated and experimental values of (**a**) U_{0mf} and (**b**) ΔP_{mf} for the dimensionless model.

Since the linear regression has better convergence ability than the nonlinear regression and does not need to assign initial values, it is more practical. Therefore, we choose the results of the linear regression method, and the final dimensionless correlation to predict U_{0mf} and ΔP_{mf} is as follows:

$$U_{0mf} = (\text{Ar})^{0.504} \cdot \left(\frac{\varepsilon_0}{\phi}\right)^{-1.355} \cdot \left(\frac{H_0}{D_0}\right)^{0.326} \cdot \left(\frac{d_P}{D_0}\right)^{0.236} \cdot \left(\frac{\theta}{R}\right)^{-0.635} \cdot \frac{\mu}{d_P \rho_g} \tag{31}$$

$$\Delta P_{mf} = (\text{Ar})^{-0.003} \cdot \left(\frac{\varepsilon_0}{\phi}\right)^{-0.642} \cdot \left(\frac{H_0}{D_0}\right)^{0.020} \cdot \left(\frac{d_P}{D_0}\right)^{0.010} \cdot \left(\frac{\theta}{R}\right)^{-0.354} \cdot \rho_s g H_0 \tag{32}$$

4.2.3. Discussion of the Two Modeling Methods

Based on the values of R^2 and RMSE of the two modeling methods (Tables 5–7), the dimensional analysis method is better than the Ergun equation modifying method. This result mainly occurs because the dimensionless correlation contains six undetermined coefficients, which is more than the three undetermined coefficients in the modified Ergun equation. More undetermined coefficients can effectively improve the fitting accuracy but also increase the complexity of the fitting calculation.

The physical laws between physical quantities are considered in the Ergun equation modifying method, so its correlation has relatively strong logicality. When using this method, by analyzing and deducing the formulas, the current fluidized state can be analyzed more deeply, and even some other inferences or conclusions can be obtained. For example, the inference of $F_{mf} = 0.8995G$ is obtained in this study, which offers some new information on analyzing the fluidized state. The dimensional analysis only fits the relationship between physical quantities from the numerical point of view. Under the condition of the same equipment and operation parameters, it has high fitting accuracy. However, the adaptability of this method is inadequate. For example, Equations (30) and (31) have higher prediction accuracy for the negative pressure conical fluidized bed with a glass bead material, but they

may not be able to predict accurately for other types of fluidized beds or materials. These two methods have their advantages and disadvantages, and the appropriate method can be chosen according to the needs of actual production.

5. Conclusions

The research equipment in this paper is a pharmaceutical conical fluidized bed with negative pressure. First, the relationship between particle size/material mass and $U_{0mf}/\Delta P_{mf}$ is explored. Then, an Ergun equation modifying method and the dimensional analysis method are used to establish prediction models for $U_{0mf}/\Delta P_{mf}$, and linear and nonlinear regression analysis methods are both used to determine the coefficients in the models. Finally, the advantages and disadvantages and applicable scope of the two modeling methods are compared and evaluated.

The conclusions of this study can be summarized as follows:

For U_{0mf}, the main influencing factor is the particle size, and the larger the particle size, the larger the U_{0mf} is; the influence of the material mass is small. For ΔP_{mf}, the main influencing factor is the material mass, and ΔP_{mf} is approximately proportional to the material mass; the influence of the particle size is relatively small. Experiments with small particles show a significant increase at large superficial gas velocity; we propose a conjecture that the particles' collision with the fluidization chamber's top surface causes this phenomenon.

The Ergun equation modifying method takes into account the physical laws between physical quantities. The original Ergun equation has low prediction accuracy for U_{0mf} and ΔP_{mf} for this study. Modifying the coefficients of the Ergun equation can significantly increase the prediction accuracy. By analyzing the data, we draw the inference of $F_{mf} = 0.8995G$, which may be due to the upward supporting effect of the conical cylinder wall on the material and needs to be further explored and verified.

The dimensional analysis method considers only the mathematical relationships between independent variables and dependent variables. Compared with the Ergun equation modifying method, the dimensional analysis method has a higher fitting accuracy. There is little difference in the fitting accuracy between the linear regression method and the nonlinear regression method.

Author Contributions: Conceptualization, S.F.; Data curation, S.F.; Formal analysis, S.F.; Investigation, S.F.; Methodology, S.F., L.F., and G.T.; Project administration, Y.W. and H.Q.; Software, L.F. and G.T.; Supervision, Y.W. and H.Q.; Validation, L.F. and G.T.; Writing—original draft, S.F. All authors have read and agreed to the published version of the manuscript.

Conflicts of Interest: The authors declare no conflict of interest.

Nomenclature

A, B	alphabetic symbols used to simplify equations, (-)
Ar	Archimedes number ($= g d_p^3 \rho_g (\rho_s - \rho_g) / \mu^2$), (-)
C_1	coefficient of the viscosity term in the Ergun equation, (-)
C_2	coefficient of the inertial term in the Ergun equation, (-)
C_3	multiplicative correction coefficient in Equation (24), (-)
d_p	particle size, (m)
F_{mf}	drag force of the incipient fluidized state, (N)
Fr	Froude number ($= U_{0mf} / \sqrt{g d_p}$), (-)
G	gravity force of particles, (N)
g	acceleration of gravity, (9.8 m/s^2)
h	height of the specified section of the conical cylinder, (m)
H	total height of particles, (m)
N	total number of points in a time-series signal, (-)
P	pressure drop, (kPa)

P_n	exponents of the dimensionless groups, (-)
r_0	radius of the bottom of the conical cylinder, (m)
r_h	sectional radius of the conical cylinder at the height of h, (m)
r_1	sectional radius of the conical cylinder at the height of H, (m)
R	Hausner ratio, (-)
Re_{mf}	Reynolds number when $U_0 = U_{0mf}$, $(= \rho_g U_{0mf} d_p / \mu)$, (-)
$RMSE_{sum}$	sum of the RMSE values of U_{0mf} and ΔP_{mf}, (-)
S_0	sectional area of the conical cylinder at the bottom, (m^2)
S_h	sectional area of the conical cylinder at the height of h, (m^2)
U_h	superficial gas velocity at the h height section of the conical cylinder, (m/s)
U_0	superficial gas velocity at the bottom section of the conical cylinder, (m/s)
U_{0mf}	minimum fluidization velocity at the bottom section of the conical cylinder, (m/s)
W	material mass, (kg)
x	discrete time-series signal, (-)
x_i	the ith value of x, (-)
$\bar{x}$	average value of x, (-)
$\hat{x}_i$	the ith calculated value of x, (-)
x_{P1}, x_{P2}	pressure time-series signal at ports P1 and P2, (Pa)
$\bar{x}_{P1}, \bar{x}_{P2}$	average value of x_{P1} and x_{P2} (Pa)
x_f	flow rate time-series signal, (L/min)
$\bar{x}_f$	average value of x_f, (L/min)
Greek letters	
α	conical angle of the conical cylinder, (°)
φ	particle sphericity, (-)
θ	angle of repose, (°)
ε	voidage of particles, (-)
ε_0	static voidage of particles, (-)
ε_{mf}	voidage of the incipient fluidized state, (-)
μ	gas viscosity, (Pa·s)
ρ_g	density of gas, (kg/m^3)
ρ_s	true density of particles, (kg/m^3)
π_n	dimensionless groups, (-)
ΔP	pressure drop between the top and bottom sections of the material, (Pa)
ΔP_{mf}	ΔP of the incipient fluidized state, (Pa)
ΔP_p	pressure drop at the gas distribution plate, (Pa)

Appendix A

Table A1. Calculated H_0 values of all experiments.

Material Number	H_0 (m)				
	Material Mass 2 kg	Material Mass 2.5 kg	Material Mass 3 kg	Material Mass 3.5 kg	Material Mass 4 kg
#1	0.0460	0.0565	0.0667	0.0765	0.0861
#2	0.0483	0.0593	0.0699	0.0802	0.0902
#3	0.0483	0.0592	0.0698	0.0801	0.0900
#4	0.0507	0.0622	0.0733	0.0840	0.0944
#5	0.0491	0.0603	0.0710	0.0815	0.0916

References

1. Shi, Y.F.; Yu, Y.S.; Fan, L.T. Incipient fluidization condition for a tapered fluidized bed. *Ind. Eng. Chem. Fundam.* **1984**, *23*, 484–489. [CrossRef]
2. Wormsbecker, M.; van Ommen, R.; Nijenhuis, J.; Tanfara, H.; Pugsley, T. The influence of vessel geometry on fluidized bed dryer hydrodynamics. *Powder Technol.* **2009**, *194*, 115–125. [CrossRef]
3. Biswal, K.C.; Sahu, S.; Roy, G.K. Prediction of the fluctuation ratio for gas-solid fluidization of regular particles in a conical vessel. *Chem. Eng. J.* **1982**, *23*, 97–99. [CrossRef]
4. Yang, W.C. Handbook of fluidization and fluid-particle systems. *China Particuol.* **2003**, *1*, 137. [CrossRef]
5. Bi, H.T. A critical review of the complex pressure fluctuation phenomenon in gas-solids fluidized beds. *Chem. Eng. Sci.* **2007**, *62*, 3473–3493. [CrossRef]
6. Biswal, K.C.; Bhowmik, T.; Roy, G.K. Prediction of minimum fluidization velocity for gas-solid fluidization of regular particles in conical vessels. *Chem. Eng. J.* **1985**, *30*, 57–62. [CrossRef]
7. Win, K.K.; Nowak, W.; Matsuda, H.; Hasatani, M.; Bis, Z.; Krzywanski, J.; Gajewski, W. Transport Velocity of Coarse Particles in Multi-Solid Fluidized Bed. *J. Chem. Eng. Jpn.* **2005**, *28*, 535–540. [CrossRef]
8. Rasteh, M.; Farhadi, F.; Bahramian, A. Hydrodynamic characteristics of gas-solid tapered fluidized beds: Experimental studies and empirical models. *Powder Technol.* **2015**, *283*, 355–367. [CrossRef]
9. Ergun, S. Fluid flow through packed columns. *Chem. Eng. Prog.* **1952**, *48*, 89–94.
10. Amiri, L.; Ghoreishi-Madiseh, S.A.; Hassani, F.P.; Sasmito, A.P. Estimating pressure drop and Ergun/Forchheimer parameters of flow through packed bed of spheres with large particle diameters. *Powder Technol.* **2019**, *356*, 310–324. [CrossRef]
11. Allen, K.G.; von Backström, T.W.; Kröger, D.G. Packed bed pressure drop dependence on particle shape, size distribution, packing arrangement and roughness. *Powder Technol.* **2013**, *246*, 590–600. [CrossRef]
12. Wen, C.Y.; Yu, Y.H. A generalized method for predicting the minimum fluidization velocity. *Aiche J.* **1966**, *12*, 610–612. [CrossRef]
13. Grace, J.R. *Handbook of Multiphase Systems*; 1982; Chapter 8.
14. Gibson, I.A.; Slim, C.J.; Zheng, Y.; Scott, S.A.; Davidson, J.F.; Hayhurst, A.N. An examination of Wen and Yu's formula for predicting the onset of fluidisation. *Chem. Eng. Res. Des.* **2018**, *135*, 103–111. [CrossRef]
15. Peng, Y.; Fan, L.T. Hydrodynamic characteristics of fluidization in liquid-solid tapered beds. *Chem. Eng. Sci.* **1997**, *52*, 2277–2290. [CrossRef]
16. Jing, S.; Hu, Q.Y.; Wang, J.F.; Jin, Y. Fluidization of coarse particles in gas-solid conical beds. *Chem. Eng. Process.* **2000**, *39*, 379–387. [CrossRef]
17. Jing, S.; Cai, G.B.; Mei, F.; Bian, Y.; Wang, J.F.; Jin, Y. Fluidization of fine particles in conical beds. *Powder Technol.* **2001**, *118*, 271–274. [CrossRef]
18. Kaewklum, R.; Kuprianov, V.I. Theoretical and experimental study on hydrodynamic characteristics of fluidization in air-sand conical beds. *Chem. Eng. Sci.* **2008**, *63*, 1471–1479. [CrossRef]
19. Koekemoer, A.; Luckos, A. Effect of material type and particle size distribution on pressure drop in packed beds of large particles: Extending the Ergun equation. *Fuel* **2015**, *158*, 232–238. [CrossRef]
20. Sau, D.C.; Mohanty, S.; Biswal, K.C. Minimum fluidization velocities and maximum bed pressure drops for gas-solid tapered fluidized beds. *Chem. Eng. J.* **2007**, *132*, 151–157. [CrossRef]
21. Sau, D.C.; Mohanty, S.; Biswal, K.C. Experimental studies and empirical models for the prediction of bed expansion in gas-solid tapered fluidized beds. *Chem. Eng. Process. Process. Intensif.* **2010**, *49*, 418–424. [CrossRef]
22. Sau, D.C.; Mohanty, S.; Biswal, K.C. Critical fluidization velocities and maximum bed pressure drops of homogeneous binary mixture of irregular particles in gas-solid tapered fluidized beds. *Powder Technol.* **2008**, *186*, 241–246. [CrossRef]
23. Khani, M.H. Models for prediction of hydrodynamic characteristics of gas-solid tapered and mini-tapered fluidized beds. *Powder Technol.* **2011**, *205*, 224–230. [CrossRef]
24. Rasteh, M.; Farhadi, F.; Ahmadi, G. Empirical models for minimum fluidization velocity of particles with different size distribution in tapered fluidized beds. *Powder Technol.* **2018**, *338*, 563–575. [CrossRef]
25. Singh, R.K.; Roy, G.K. Prediction of minimum bubbling velocity, fluidization index and range of particulate fluidization for gas-solid fluidization in cylindrical and non-cylindrical beds. *Powder Technol.* **2005**, *159*, 168–172. [CrossRef]

26. Hosseini, S.H.; Rezaei, M.J.; Bag-Mohammadi, M.; Karami, M.; Moradkhani, M.A.; Panahi, M.; Olazar, M. Estimation of the minimum spouting velocity in shallow spouted beds by intelligent approaches: Study of fine and coarse particles. *Powder Technol.* **2019**, *354*, 456–465. [CrossRef]

27. Hosseini, S.H.; Karami, M.; Olazar, M.; Safabakhsh, R.; Rahmati, M. Prediction of the Minimum Spouting Velocity by Genetic Programming Approach. *Ind. Eng. Chem. Res.* **2014**, *53*, 12639–12643. [CrossRef]

28. Gan, L.; Lu, X.; Wang, Q. Experimental and theoretical study on hydrodynamic characteristics of tapered fluidized beds. *Adv. Powder Technol.* **2014**, *25*, 824–831. [CrossRef]

29. Golshan, S.; Yaman, O.; Koksal, M.; Kulah, G.; Zarghami, R.; Mostoufi, N. A new correlation for minimum spouting velocity for conical spouted beds operating with high density particles. *Exp. Therm. Fluid Sci.* **2018**, *96*, 358–370. [CrossRef]

30. Hosseini, S.H.; Rezaei, M.J.; Bag-Mohammadi, M.; Altzibar, H.; Olazar, M. Smart models to predict the minimum spouting velocity of conical spouted beds with non-porous draft tub. *Chem. Eng. Res. Des.* **2018**, *138*, 331–340. [CrossRef]

31. Murthy, J.S.N.; Reddy, V.S.; Tasleem, S.; Kumar, D.V.; Krishna, C.S.; Sankarshana, T. Hydrodynamics of gas-solid fluidization in tapered beds. *Can. J. Chem. Eng.* **2009**, *87*, 359–374. [CrossRef]

32. Van Ommen, J.R.; Schouten, J.C.; Vander Stappen, M.L.M.; Bleek, C.M.V.D. Response characteristics of probe-transducer systems for pressure measurements in gas-solid fluidized beds: How to prevent pitfalls in dynamic pressure measurements. *Powder Technol.* **1999**, *106*, 199–218. [CrossRef]

33. Geldart, D. Types of gas fluidization. *Powder Technol.* **1973**, *7*, 285–292. [CrossRef]

34. Schaafsma, S.H.; Marx, T.; Hoffmann, A.C. Investigation of the particle flowpattern and segregation in tapered fluidized bed granulators. *Chem. Eng. Sci.* **2006**, *61*, 4467–4475. [CrossRef]

35. Gernon, T.M.; Gilbertson, M.A. Segregation of particles in a tapered fluidized bed. *Powder Technol.* **2012**, *231*, 88–101. [CrossRef]